Sparsity-Enforced Joint Spiral Trajectory & RF Excitation Pulse Design

A. C. ZELINSKI[1], V. K. GOYAL[1], L. L. WALD[2,3], AND E. ADALSTEINSSON[1,3]

[1]RESEARCH LABORATORY OF ELECTRONICS, MIT, CAMBRIDGE, MA, UNITED STATES, [2]MARTINOS CENTER FOR BIOMEDICAL IMAGING, HARVARD MEDICAL SCHOOL, MGH, CHARLESTOWN, MA, UNITED STATES, [3]HARVARD-MIT DIVISION OF HEALTH SCIENCES & TECHNOLOGY, CAMBRIDGE, MA, UNITED STATES

INTRODUCTION. Algorithms have recently been proposed that jointly optimize excitation *k*-space trajectories & RF excitation pulses [1-4]. Each relies on a small-tip-angle assumption and has been shown to produce higher-quality excitations or shorter excitation pulses than conventional 3D spoke-based [1,2], 2D echo-planar (EP) [3], and 2D spiral trajectories [4]. Here we propose a sparsity-enforcement algorithm that jointly determines sparse, quickly-traversable *k*-space trajectories and excitation pulses. The method is applicable to single- as well as multi-channel transmission systems. An L_1 penalty is used when searching over a large number of possible trajectory segments to reveal a small subset of these segments (along with an RF pulse) that *alone* form a high-fidelity version of a user-specified target excitation. These segments may be of any shape or size, but here, we provide the algorithm with *candidate rings* in *k*-space, thus focusing on the optimization of spirals. Simulations are conducted using data from a single-channel 7T system: for a Gaussian-shaped target and inhomogeneous transmit profile, we show that sparsity-enforced spirals lead to improvements in both excitation quality & pulse duration relative to conventional radially-undersampled ("accelerated") spirals.

Fig. 1: Transmit Profile & Desired Magnetization

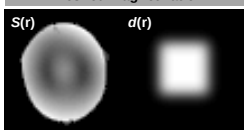

Fig. 2: Candidate Rings, Sparsity-Enforced 4-Ring Subset, and Resulting 1.5 ms Trajectory

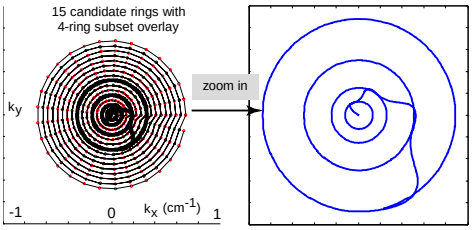

METHODS. **Transmission profile & desired target magnetization pattern**. Fig. 1 depicts the transmit profile, $S(\mathbf{r})$, of a birdcage coil in a water phantom at 7T, along with the desired magnetization pattern, $d(\mathbf{r})$. Forming $d(\mathbf{r})$ in the presence of the inhomogeneous $S(\mathbf{r})$ is non-trivial.

Conventional spirals. Consider a spiral whose radii are spaced at the Nyquist-limit (as defined by the desired FOV). Defining an unaccelerated Nyquist-sampled spiral an "R=1" spiral, the conventional way to sparsify (accelerate) the trajectory is to radially undersample its rings by a factor of R. This process does indeed accelerate the trajectory and reduce pulse duration, but does not explicitly take the desired magnetization pattern into account.

Sparsity-enforced spiral design. We develop a spiral acceleration method that accounts for $d(\mathbf{r})$ up-front and determines *target-specific* trajectory-pulse combinations. We start by deriving the algorithm for a single-channel system. Imagine C contours (e.g., ellipses, rings) in *k*-space; for each contour c, N_c *k*-space locations along the contour are known: $\mathbf{k}_{c,1}, \ldots, \mathbf{k}_{c,Nc}$. Overall, $N_k = N_1 + \cdots + N_C$ discrete *k*-space points are known. The goal is to find the *smallest contour subset* along with a corresponding pulse such that when the pulse is played along the path defined by the small set of contours, a high-fidelity version of $d(\mathbf{r})$ is produced; the contour segments in the small subset may then be connected via gradients to yield a highly-sparse, fast *k*-space trajectory. We pose an optimization that seeks an energy weighting to place in *k*-space to form $d(\mathbf{r})$, but where a penalty is incurred whenever a contour experiences a nonzero energy deposition. This ensures only a small number of contours will be used. First, the linearized formalism of [5] is applied, allowing us to relate energy placed along each *k*-space contour to the resulting magnetization, $m(\mathbf{r})$: $\mathbf{m} = \mathbf{SC}_1\mathbf{g}_1 + \cdots + \mathbf{SC}_C\mathbf{g}_C = \mathbf{A}_{tot}\mathbf{g}_{tot}$ (Eq. 1), where $\mathbf{m} \in \mathcal{C}^{Ms}$ contains samples of $m(\mathbf{r})$ at $\mathbf{r}_1, \ldots, \mathbf{r}_{Ms}$, $\mathbf{S} \in \mathcal{C}^{Ms \times Ms}$ is a matrix of $S(\mathbf{r})$ samples, & $\mathbf{g}_c \in \mathcal{C}^{Nc}$ contains weights the transmit channel places at the N_c *k*-space locations of contour c. Each $\mathbf{C}_c$ relates how energy placed along contour c affects the resulting excitation: formally, $\mathbf{C}_c(u,v) = j\gamma\Delta_t \cdot M_0 \cdot \exp(j\mathbf{r}_u \cdot \mathbf{k}_{c,v})$, $\mathbf{C} \in \mathcal{C}^{Ms \times Nc}$, $\mathbf{A}_{tot} = [\mathbf{SC}_1 \cdots \mathbf{SC}_C]$, & $\mathbf{g}_{tot} = [\mathbf{g}_1^T \cdots \mathbf{g}_C^T]^T$. The desired excitation, $d(\mathbf{r})$, is vectorized to $\mathbf{d} \in \mathcal{C}^{Ms}$. Solving $\mathbf{d} = \mathbf{A}_{tot}\mathbf{g}_{tot}$ (Eq. 2) for $\mathbf{g}_{tot}$ via the pseudoinversion of $\mathbf{A}_{tot}$ results in a solution where energy is placed along *all* contours, i.e., all $\|\mathbf{g}_c\|_2$s are nonzero, failing to reveal a useful contour subset. Consider however solving Eq. 2 while penalizing each nonzero contour energy (each $\|\mathbf{g}_c\|_2$), which prohibits the use of many contours while encouraging those that remain to form $\mathbf{g}_c$s that approximately solve Eq. 2. This is accomplished by solving $\min_{\mathbf{G}} \{\|\mathbf{d} - \mathbf{A}_{tot}\mathbf{g}_{tot}\|_2^2 + \lambda \cdot \sum_c (\|\mathbf{g}_c\|_2)\}$ (Eq. 3) for fixed λ, where $\sum_c(\|\mathbf{g}_c\|_2)$ is the L_1-norm of the $\|\mathbf{g}_c\|_2$ contour energies; such a norm encourages sparsity [6,7]. As λ:0→1, increasing numbers of contours have their energies driven to zero, residual error increases, and smaller contour subsets are revealed. For $N_k < 1000$, finding a small contour subset takes only several minutes. After solving Eq. 3 for a large λ, an optimized Q-contour subset is formed, comprised of those Q contours whose $\|\mathbf{g}_c\|_2$s are largest. The Q segments are then connected via an in-house method, yielding $\mathbf{k}(t)$ & $\mathbf{G}(t)$. Finally, the RF pulse is retuned by truncating $\mathbf{A}_{tot}$ & $\mathbf{g}_{tot}$ and least-squares fitting to Eq. 2. For a P-channel parallel transmission system, $\mathbf{A}_{tot}$ of Eq. 1 will contain PC rather than C submatrices, there will be PC $\mathbf{g}_{p,c}$ weight vectors, and Eq. 3's regularization term becomes $\sum_c(\|[\mathbf{g}_{1,c}^T \cdots \mathbf{g}_{P,c}^T]^T\|_2)$, i.e., only *overall* contour energy is penalized; whether it is one channel or all channels that make large contributions to a contour does not matter if the use of this contour greatly helps at forming the excitation.

Fig. 3: Sparsity-Enforced 4-Ring RF Pulse and Gradients

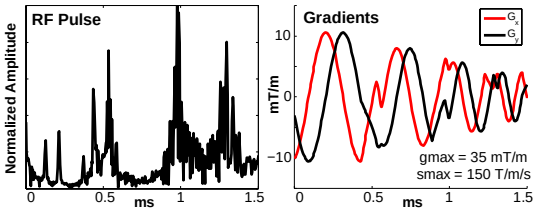

Fig. 4: Excitations due to Sparsity-Enforced & Accelerated Spirals

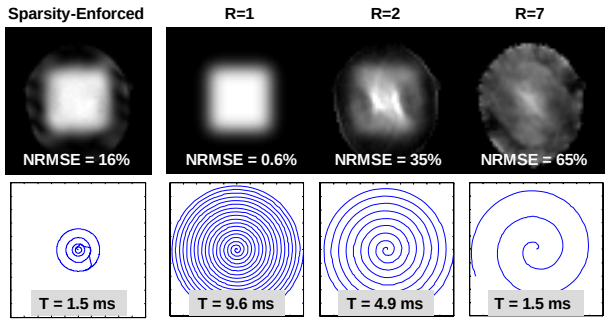

RESULTS. A sparsity-enforced spiral trajectory and RF pulse are designed by first defining the $C = 16$ contours shown in the left panel of Fig. 2; there are 15 candidate rings, each comprised of 25 *k*-space points, along with a single point at DC (thus $N_k = 376$). These contours, along with $S(\mathbf{r})$ and $d(\mathbf{r})$, are provided to the method, λ is set to 0.30, and Eq. 3 is then solved in under 2 minutes. Four rings are retained as the sparsity-enforced subset and appear as overlays on the left panel of Fig. 2. The right panel of Fig. 2 shows how the 4-ring subset is connected into a 1.5-ms trajectory, and Fig. 3 depicts the corresponding gradients and retuned RF pulse. Fig. 4 compares excitations due to the sparsity-enforced spiral and R-accelerated conventional spirals. The 1.5-ms sparsity-enforced spiral significantly outperforms the 4.9-ms, $R = 2$ spiral. The $R = 1$ spiral does indeed produce a near-perfect excitation, but is 6.4x longer than the optimized pulse. Note how the sparsity-enforced spiral traverses only a small segment of *k*-space yet is capable of forming a high-fidelity version of the box, in spite of the presence of the inhomogeneous $S(\mathbf{r})$. When $R = 7$, the conventionally-accelerated spiral has a duration on-par with the optimized spiral, but has 4x larger error. Thus for fixed excitation quality, the sparsity-enforced spiral yields shorter pulses, and for fixed pulse duration, it yields lower-NRMSE excitations.

CONCLUSION. A spiral trajectory acceleration algorithm based on sparsity-enforcement concepts has been shown to rapidly calculate fast, high-quality trajectories & corresponding RF pulses. Sparsity-enforced spiral trajectories significantly outperformed conventional spirals in simulated trials in a single-channel, 7T, non-uniform transmit profile setting.

REFERENCES. [1] Setsompop, Zelinski et al. ISMRM '07, p 356. [2] Zelinski et al. ISMRM '07, p 1691. [3] Yip et al. MRM '07:58(3);598-604. [4] Levin et al. ISMRM '06, p 3012. [5] Grissom et al. MRM. 2006;56(3):620-629. [6] Chen et al. SIAM Rev '01;43(1):129–159. [7] Malioutov et al. IEEE Trans Sig Proc '05;53(8).